ARTICLE | Article in Press

Multi-domain feature fusion and machine learning-based SFRA diagnosis of transformer winding faults using a novel fault deviation index

Cemal Keleş · Mehmet Salih Mamiş · Müslüm Arkan · Murat Köseoğlu · Zehva Yalçınöz

Received: 18 May 2026 / Accepted: 16 September 2026
© The Author(s) 2026

Abstract
Sweep Frequency Response Analysis (SFRA) is one of the commonly used techniques for evaluating transformer winding integrity. However, the interpretation of the SFRA results remains qualitative and depends on expert evaluation. In this study, a quantitative, measurement-oriented diagnostic framework based on the advanced normalized Multi-Domain Fault Deviation Index (MFDI) is proposed. Within this method, magnitude, phase, impedance, and resonance-based descriptors are integrated in a unified formulation. The proposed method combines frequency band decomposition with multi-domain feature fusion to capture both local and global spectral deviations. This framework is experimentally validated under both intra-phase (U–N) and inter-phase (V–W) fault scenarios using SFRA measurements. The results demonstrate that the proposed MFDI captures the obvious difference between healthy and faulty states. For intra-phase fault scenarios, the proposed method provides quantitative differentiation among the investigated fault conditions despite the high similarity of their corresponding spectral signatures. In contrast, inter-phase faults generate more pronounced global spectral deviations, leading to highly separable feature representations for Support Vector Machine (SVM) and Random Forest (RF) classifiers. These findings demonstrate that the proposed approach advances SFRA from a predominantly qualitative interpretation technique toward a quantitative, interpretable, and machine-learning-compatible diagnostic methodology suitable for intelligent transformer condition monitoring.

Keywords Transformer winding fault diagnosis · SFRA · Multi-domain feature fusion · MFDI · Machine learning

Introduction

Sustainable and reliable electrical energy supply is one of the most essential requirements of modern society. Power transformers are among the most critical and indispensable components of electrical power systems[1]. Faults in power transformers can cause lengthy power outages, disruptions in system stability, and significant financial losses. Therefore, early detection of transformer faults is of great importance[2,3].

This Article in Press is shared early to give you faster access to new research. It is citable and carries a permanent DOI. The final edited version will replace it automatically.

https://doi.org/10.1038/s41598-026-72481-3

Published online: 25 September 2026

scientific reports

Significant proportion of transformer faults have been reported to originate from mechanical and electrical degradation in the windings[2,4]. Changes in winding geometry may arise from electromechanical force, switching transients, thermal aging, insulation degradation, and prolonged operating conditions[5]. These structural changes may develop into serious internal faults, directly threatening the safe operation of the transformer[6–8].

For many years, traditional diagnostic methods such as insulation resistance measurement, winding transformation ratio testing, partial discharge analysis, dielectric loss measurement, and dissolved gas analysis have been widely used for the detection of transformer faults[9,10]. However, these methods do not always provide sufficient sensitivity to identify local mechanical disturbances or incipient deformations in the transformer windings. Consequently, there has been an increasing demand for alternative diagnostic techniques capable of detecting subtle changes in the electromechanical structure of transformers[10–12].

In recent years, frequency-based diagnostic methods that provide sensitive responses to changes in the internal structure of transformers have attracted considerable attention[13]. Among these methods, Sweep Frequency Response Analysis (SFRA), is a reliable and widely accepted method for evaluating transformer winding integrity[4,14,15]. This approach, first introduced by Dick and Erven (1978)[16], is based on measuring the electrical response of the transformer over a wide frequency range[17]. Subsequent studies have shown that SFRA is highly effective in determining mechanical deformations, axial and radial displacement, inter-turn faults, and various internal structural anomalies[3,6,18,19]. In particular, changes in magnitude behavior, deviations in phase response, variations in impedance characteristics, and shifts in resonance frequencies provide important diagnostic information regarding internal coil structural abnormalities[7,10,20,21].

Several studies in the literature have investigated the measurement configurations, physical foundations, and fault mechanisms of SFRA in power transformers. Alsuhaibani et al.[10] comprehensively addressed SFRA-based diagnostic methods and examined the effects of different fault types on the frequency response characteristics of transformers. Senobari et al.[7] considered SFRA as an advanced diagnostic tool providing information regarding the nature and location of the transformer faults.

Despite these advantages, the use of SFRA in industrial applications largely relies on comparative analysis of magnitude and phase response curves. In many cases, differences between the healthy and current state frequency response curves are evaluated. However, this approach has significant limitations, such as subjective interpretation, difficulty in standardization, and the inability to be directly integrated into automated condition monitoring systems[22,23].

To overcome the limitations associated with interpreting differences between frequency response curves, various approaches such as correlation-based similarity measures, quality indices, resonance shift-based descriptors, statistical approaches, and multiple decision mechanisms have been proposed[17]. In particular, the frequency response quality indices proposed by Kornatowski and Banaszak[24] have been shown to contribute to a more systematic evaluation of the mechanical distortions in transformer windings. Similarly, Samimi and Tenbohlen[11] developed indices that can quantitatively express the differences between SFRA curves. Al-Ameri et al.[22] drew attention to the necessity of multiband and multidimensional analysis approaches in different frequency regions in SFRA interpretation.

In recent years, machine learning-based approaches have also shown significant progress in the field of SFRA for fault classification[25,26]. Zhao et al.[27] demonstrated that transformer winding faults can be classified using Support Vector Machines (SVM) on online IFRA data. Zhang et al.[28] proposed a dimensionality reduction-supported hierarchical classification model to identify first-stage winding faults. Tahir et al.[29] developed a situation assessment approach based on artificial neural networks. In a subsequent study, Tahir et al.[30] improved the performance of automatic interpretation using a Random Forest-based model. In addition to these studies, significant improvements in fault localization and classification accuracy from SFRA data have been reported using deep learning, hybrid feature extraction, and image processing-based methods[31–33].

Taken together, previous studies show that SFRA contains considerably more diagnostic information than can be obtained from visual curve comparison alone. A key challenge in SFRA analysis is to quantify the differences

between healthy and faulty responses while retaining their physical meaning. This is particularly important because fault-related information may appear in different response domains and frequency regions. To address this issue, the present study introduces the Advanced Normalized Multi-Domain Fault Deviation Index (MFDI), which brings these complementary features together in a single quantitative representation. Magnitude, phase, impedance, impedance-phase, and resonance-related information are evaluated together, while frequency-band decomposition is used to retain local spectral changes. Machine-learning models are then used to examine whether the resulting feature representation can distinguish the investigated transformer conditions. Classification is used here as a validation step rather than as the main contribution of the study. The experiments in this study focus on the selected intra-phase and inter-phase short-circuit conditions. Therefore, the method is evaluated in terms of its ability to distinguish these conditions from the healthy state and from each other. Estimating the degree of mechanical winding deformation or determining the exact location of a fault is beyond the scope of the present study.

Methodology

SFRA-based transformer modeling

In SFRA, the transformer winding can be represented by a distributed RLC network whose electrical response varies with frequency. The measured transfer function is expressed as

$$H(f) = \frac{V_o(f)}{V_i(f)} \tag{1}$$

where, $H(f)$ denotes the frequency response function, and $V_i(f)$ and $V_o(f)$ are the applied and measured voltages, respectively. Changes in the winding structure alter the effective resistance, inductance, capacitance, and coupling within this distributed network. As a result, mechanical or electrical faults may appear as changes in the magnitude and phase responses, impedance characteristics, or resonance pattern of the winding.

Multi-domain feature representation

A single SFRA response quantity does not fully describe the electrical changes produced by a winding fault. For this reason, four complementary response domains are considered in the proposed framework: magnitude $M(f)$, phase $P(f)$, impedance $Z(f)$, and impedance phase $\Phi_Z(f)$. These quantities reflect different aspects of the winding response. Magnitude and phase describe the transfer characteristics of the system. Although the impedance-based quantities are more directly related to changes in the equivalent electrical parameters of the winding.

To determine the deviations between healthy and malfunctioning states, a normalized difference is defined for each domain. This normalization is necessary to account for the contribution of all domains, regardless of their values or units.

To compare these domains within the same diagnostic framework, the difference between the healthy and faulted responses is normalized separately for each quantity. The corresponding deviations are defined as

$$d_M(f) = \frac{|M_f(f) - M_h(f)|}{\sigma_M} \tag{2}$$

$$d_P(f) = \frac{|P_f(f) - P_h(f)|}{\sigma_P} \tag{3}$$

$$d_Z(f) = \frac{|\log|Z_f(f)| - \log|Z_h(f)||}{\sigma_Z} \tag{4}$$

$$d_{\Phi}(f) = \frac{|\Phi_f(f) - \Phi_h(f)|}{\sigma_{\Phi}} \tag{5}$$

where the subscripts h and f denote the healthy and faulted conditions, respectively. The parameters σ_M, σ_P, σ_Z, and σ_{Φ} are the standard deviations of the corresponding healthy state responses. This normalization reduces the influence of differences in scale and units and prevents a single response domain from dominating the combined index.

The impedance magnitude covers a considerably wider numerical range than the other SFRA quantities. For this reason, the impedance deviation is evaluated on a logarithmic scale. This reduces the influence of large impedance values and allows impedance-related changes to be considered together with magnitude, phase, and impedance-phase variations on a more balanced basis.

Frequency band decomposition

The diagnostic information contained in an SFRA trace is not distributed uniformly over the frequency range. Different parts of the spectrum are influenced by different electromagnetic properties of the transformer[34]. At low frequencies, the response is governed mainly by the magnetic core and the overall winding inductance. As frequency increases, winding geometry, mutual coupling, and local structural changes become more influential. In the high-frequency region, distributed capacitances dominate the response, while localized discontinuities may appear through changes in resonance behavior and capacitive coupling. Leakage inductance remains part of the equivalent network, although its relative influence becomes smaller in this region compared with the distributed capacitive effects[7,10].

To retain these frequency-dependent characteristics, the SFRA spectrum is divided into b contiguous bands,

$$F_b = [f_b, f_{b+1}] \qquad b = 1,2,\ldots,B \tag{6}$$

where B is the number of frequency bands and f_b and f_{b+1} define the lower and upper limits of the b-th band. In the present study, four ranges were used: 20 Hz–1 kHz, 1–10 kHz, 10–100 kHz, and 100 kHz–2 MHz. These limits were selected to remain consistent with the conventional physical interpretation of SFRA responses reported in the literature[3,6,7,10,16]. The first band is mainly associated with core and overall inductive behavior, the two intermediate bands are more responsive to changes in winding geometry and coupling, and the highest-frequency band is dominated primarily by distributed capacitances and local structural effects.

Rather than extracting features from the entire spectrum as a single response, the analysis is performed separately within each band. This preserves local variations that could otherwise be averaged out in a full-spectrum comparison. Figure 1 illustrates the adopted decomposition using the intra-phase (U–N) response as an example. The same frequency limits were used for the inter-phase (V–W) measurements.

Each band was further divided into six non-overlapping windows. Magnitude, phase, impedance, impedance-phase, resonance, correlation, centroid, and local MFDI descriptors were then calculated within each window. The resulting local descriptors form the feature vectors used in the subsequent quantitative and machine-learning analyses.

For each sub-band, representative descriptors are obtained by summing the normalized deviations. The mean magnitude deviation is defined as follows:

$$E_M^{(b)} = \frac{1}{N_b} \sum_{f_k \in F_b} d_M(f_k) \tag{7}$$

Here, N_b is the number of frequency samples in the b-th band, $d_M(f_k)$ is the normalized magnitude deviation at frequency f_k. Similarly, $E_P^{(b)}$, $E_Z^{(b)}$, and $E_{\Phi}^{(b)}$ are the phase, impedance, and impedance-phase deviation, respectively. This band-based decomposition improves robustness by reducing local fluctuations. Thus, this method makes it possible to capture frequency-based fault effects[3,7].

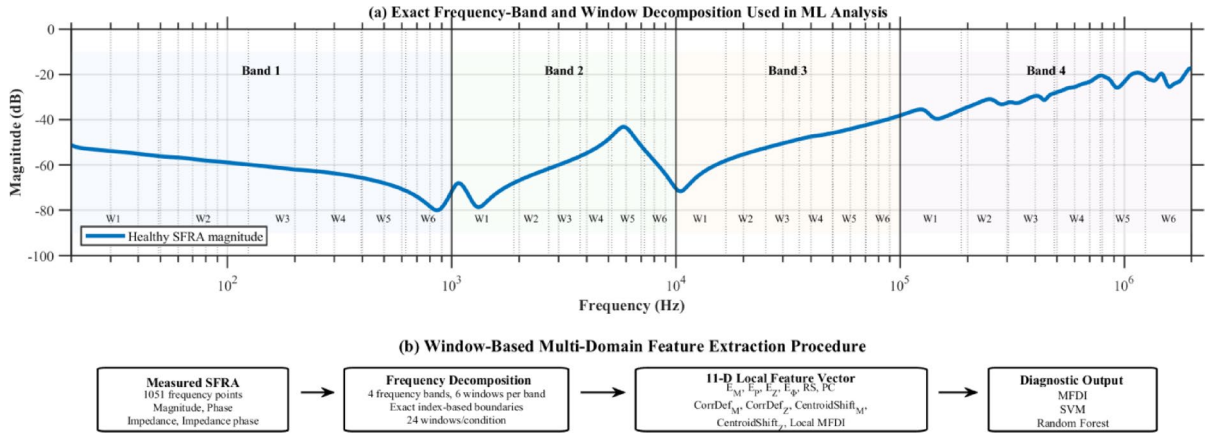


Fig. 1 (**a**) Representative illustration of the frequency-band decomposition and (**b**) window-based feature extraction procedure using the intra-phase (U–N) SFRA response.

Resonance-based descriptor

As a reliable indicator of winding deformations and physical changes in the transformer's internal structure, changes occurring in resonance frequencies are accepted as a key feature[6,7]. The relative shift in resonance frequency is defined to express this change numerically in Eq. (8).

$$RS^{(b)} = \frac{1}{N_r} \sum_{i=1}^{N_r} \frac{\left| f_{r,i}^{(f)} - f_{r,i}^{(h)} \right|}{f_{r,i}^{(h)}} \tag{8}$$

Here, $f_{r,i}^{(h)}$ and $f_{r,i}^{(f)}$ represent the i-th resonance frequencies under healthy and faulted conditions, respectively. N_r is the number of detected resonances. This measurement determines the normalized shift in resonance frequencies.

In addition to shifts in resonance frequencies, changes in the number of resonance peaks also provide important diagnostic information. Such changes are often associated with winding displacement or short-circuit faults[22]. Therefore, the change in the number of peaks is defined as follows:

$$PC^{(b)} = \left| N_r^{(f)} - N_r^{(h)} \right| \tag{9}$$

Here, $N_r^{(h)}$ and $N_r^{(f)}$ correspond to the number of peaks detected in healthy and faulty responses, respectively. Both the resonance shift and change in peak number provide a complementary perspective on structural variations.

Spectral correlation and centroid features

Correlation-based SFRA indices have been widely adopted to quantify waveform similarity and enhance objectivity of interpretation[11,24]. Two complementary descriptors are incorporated to improve sensitivity to global spectral variations[21].

Correlation deficit

The similarity between healthy and faulted signals is quantified using the Pearson correlation coefficient:

$$CD = 1 - r\left(X_f, X_h\right) \tag{10}$$

Here, r is the Pearson correlation coefficient. X_h and X_f are healthy and faulted signals, respectively.

Spectral centroid shift

The spectral centroid represents the distribution of energy across the frequency spectrum:

$$C = \frac{\sum f \cdot \mid X(f) \mid}{\sum \mid X(f) \mid} \tag{11}$$

The normalized shift is defined as follows:

$$CS = \frac{\mid C_f - C_h \mid}{C_h} \tag{12}$$

Here, C_h and C_f are centroids of healthy and faulted responses, respectively.

Proposed MFDI formulation

The proposed MFDI integrates all descriptors into a unified index:

$$\text{MFDI} = \sum_{b=1}^{B} \alpha_b \left(w_M E_M^{(b)} + w_P E_P^{(b)} + w_Z E_Z^{(b)} + w_\Phi E_\Phi^{(b)} + w_{RS} RS^{(b)} + w_{PC} PC^{(b)} \right) \tag{13}$$

where α_b is the band weight, w_* are the feature weights, $E_*^{(b)}$ are the band-wise deviations. $RS^{(b)}$ and $PC^{(b)}$ are the resonance descriptors, respectively.

Weight selection strategy

The MFDI combines multiple response domains and frequency bands, each contributing differently to transformer fault characterization. Feature weights were determined by considering the response of SFRA signals to faults. Higher weights were given to magnitude and impedance characteristics, which are more sensitive to structural changes. Phase and resonance characteristics were considered as components providing complementary information.

Normalization was applied to ensure balanced contribution from all features. Fisher-type analysis is also used to determine the effectiveness of feature weights[35]. In this study, the discriminative power of the features was examined using this analysis. It was observed that magnitude and impedance provided strong information, whereas phase and resonance provided supporting information. Thus, the proposed index offers a robust structure capable of meaningfully evaluating faults both numerically and physically.

Machine learning integration

In recent years, machine learning has been increasingly applied in fault diagnosis studies using SFRA data[27–29,36]. The main purpose is to automatically classify faults and increase the accuracy rate. However, the performance of these methods depends on the characteristics and physical interpretability of the extracted features. Therefore, this study prioritizes physically based features and employs machine learning models to evaluate the effectiveness of these features.

Each experimentally measured SFRA response consisted of 1051 frequency points covering 20 Hz–2 MHz, with magnitude, phase, impedance, and impedance-phase values recorded at each point. Using the frequency-band and window decomposition described in Sect. 2.3, 24 non-overlapping frequency windows were obtained from each measured SFRA response. An 11-dimensional local feature vector comprising magnitude, phase, impedance and impedance-phase deviations, resonance shift, peak-count variation, correlation deficits, spectral centroid shifts, and the local MFDI was extracted from each window. This procedure generated 24 window-based feature vectors per measured operating condition. For the intra-phase analysis, four balanced classes (healthy, 3U–4U,

4U–5U, and 2U–3U short circuit) yielded 96 feature vectors in total. For the inter-phase analysis, the healthy and 4 V–2 W short-circuit conditions yielded 48 feature vectors, with 24 vectors in each class. These feature vectors represent frequency-window observations derived from the experimentally measured SFRA responses and should not be interpreted as independent transformer experiments.

To evaluate the discriminative capability of the proposed multi-domain feature set, Support Vector Machine (SVM) and Random Forest (RF) classifiers were employed. For the intra-phase analysis, multiclass classification was implemented using an Error-Correcting Output Codes (ECOC) framework with one-versus-all SVMs and an RBF kernel (KernelScale = auto). The same classifier settings were adopted for the inter-phase analysis. Random Forest classification was performed using bagged decision trees with 100 learning cycles and a maximum of 20 splits per tree. Prior to classification, all feature vectors were standardized using z-score normalization. Model performance was evaluated using five-fold cross-validation[37]. Hyperparameters were selected using the default MATLAB R2023b settings, and no additional hyperparameter optimization was performed because the objective of the machine-learning analysis was to evaluate the discriminative capability of the proposed physically based feature representation rather than to maximize classification accuracy.

Each sample is represented as follows:

$$x = \left[E_M^{(b)}, E_P^{(b)}, E_Z^{(b)}, E_\Phi^{(b)}, RS^{(b)}, PC^{(b)}, CD, CS\right] \tag{14}$$

Prior to classification, features are standardized using z-score normalization:

$$x' = \frac{x - \mu}{\sigma} \tag{15}$$

Here, μ represents the mean and σ denotes the standard deviation.

For clarity and reproducibility, the composition of the machine-learning dataset, the feature extraction strategy, the validation procedure, and the classifier configurations adopted in this study are summarized in Table 1.

The computational complexity of the proposed framework was also considered in terms of both feature extraction and classification. Let N denote the number of frequency points in an SFRA measurement ($N = 1051$ in this study). The normalized deviations in the magnitude, phase, impedance, and impedance-phase domains are computed directly over the measured frequency points and therefore require O(N) operations. Since the subsequent

Table 1 Summary of the machine learning dataset and classifier configuration.

Parameter	Intra-phase (U–N)	Inter-phase (V–W)
Frequency range	20 Hz–2 MHz	20 Hz–2 MHz
Frequency points per SFRA measurement	1051	1051
Measured domains	Magnitude, Phase, Impedance, Impedance Phase	Magnitude, Phase, Impedance, Impedance Phase
Frequency bands	4	4
Windows per band	6	6
Operating conditions	Healthy, 3U–4U, 4U–5U, 2U–3U	Healthy, 4 V–2 W
Feature vectors per operating condition	24	24
Total feature vectors	96	48
Class distribution	24 / 24 / 24 / 24	24 / 24
Feature normalization	Z-score	Z-score
Validation strategy	5-fold cross-validation	5-fold cross-validation
SVM configuration	ECOC (One-vs-All), RBF kernel, KernelScale = auto	RBF kernel, KernelScale = auto
Random Forest configuration	Bagging, 100 trees, MaxNumSplits = 20	Bagging, 100 trees, MaxNumSplits = 20
Software	MATLAB R2023b	MATLAB R2023b
Feature vector dimension	11	11

band- and window-based statistical descriptors are extracted from non-overlapping subsets of the same spectrum, their overall computational cost also scales approximately linearly with N. Resonance-related features involve peak-detection operations within individual windows; therefore, their exact computational cost is implementation-dependent, although the number of processed frequency points remains bounded by N. Consequently, the overall feature-extraction stage scales approximately as O(N) with respect to the SFRA data length. The extracted feature vector has a fixed dimension of 11, and the classification stage operates on 96 and 48 feature vectors for the intra-phase and inter-phase analyses, respectively. Thus, for the datasets considered in this study, the dimensionality and sample size of the classification problem remain relatively small, resulting in a limited computational burden and supporting the feasibility of the framework for offline transformer condition assessment.

Results and discussion

Experimental setup and data acquisition

The proposed MFDI framework was evaluated through controlled laboratory experiments using the transformer and SFRA measurement system. Figure 2 illustrates the transformer winding terminals and the connections used in the experiments. U, V, and W represent the three high-voltage winding phases, while N represents the neutral terminal. The numbered terminals indicate the specific points along the windings used to establish the measurement and fault configurations.

The predefined terminals shown in Fig. 2 were also used to introduce the investigated short-circuit conditions. For the intra-phase tests, short circuits were applied between terminals 2U–3U, 3U–4U, and 4U–5U. These winding sections contain 110, 330, and 110 turns, respectively, as indicated in Fig. 2. The inter-phase fault was introduced by connecting terminals 4 V and 2 W. Accordingly, the experimental cases represent different short-circuit locations and winding sections rather than controlled levels of mechanical deformation. For this reason, no percentage of winding displacement or mechanical deformation severity was assigned to the investigated fault conditions.

The complete measurement arrangement is shown in Fig. 3. It includes the test transformer, FRAX 101 frequency response analyzer, shielded connection cables, grounding system, and data-acquisition computer. Measurements were carried out under controlled laboratory conditions to reduce the influence of external electromagnetic interference. The FRAX 101 applied a low-amplitude sinusoidal sweep over the specified frequency range, as illustrated in Fig. 4.

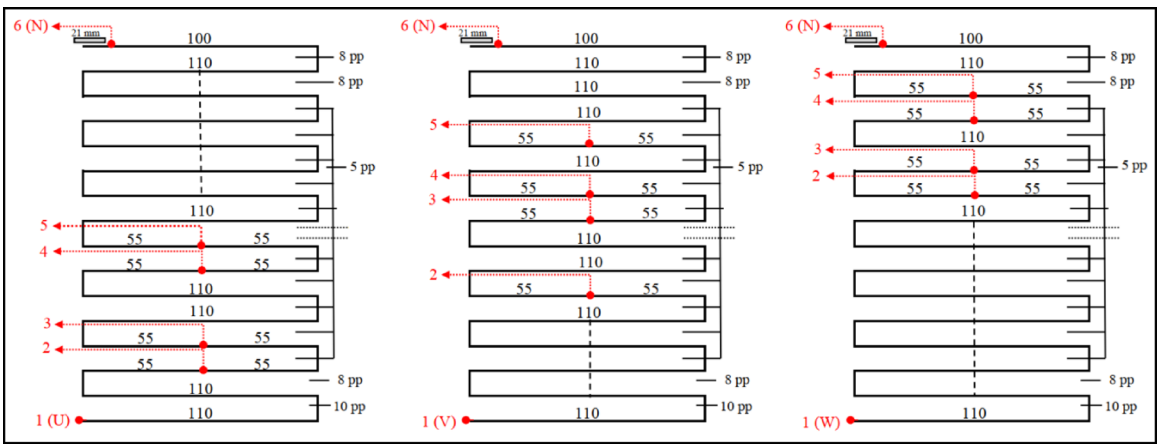


Fig. 2 Schematic representation of the transformer winding terminals and connection points used in the SFRA experiments.

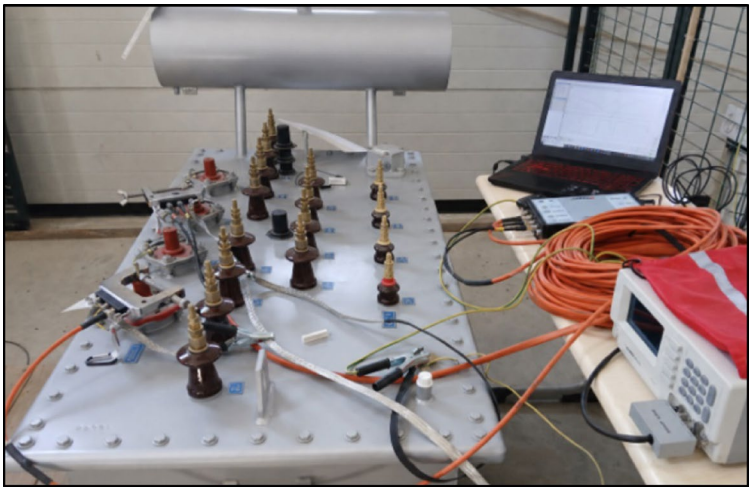


Fig. 3 Experimental setup for transformer SFRA measurements.

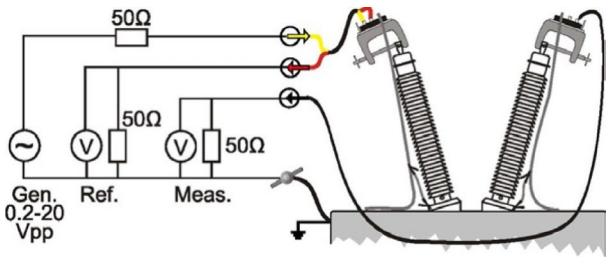


Fig. 4 Frequency response measurement setup and data acquisition framework for transformer SFRA analysis[38].

Table 2 Transformer specifications and SFRA measurement parameters.

Category	Parameter	Value / Description
Transformer	Rated power	50 kVA
	Rated voltage	10 kV / 0.4 kV
	Phase configuration	Three-phase
	Winding type	Copper windings
	Cooling method	Oil-cooled
	Frequency (nominal)	50 Hz
SFRA measurement	Frequency range	20 Hz – 2 MHz
	Measurement device	FRAX 101 Frequency Response Analyzer
	Excitation signal	Low-voltage sinusoidal sweep
	Input voltage level	10 V (peak)
	Measurement mode	End-to-end / End-to-ground (specify per test)
Connection setup	Grounding	Transformer tank and reference grounded
	Cable type	Shielded coaxial cables
	Connection repeatability	Fixed connection points for all tests
Fault configuration	Fault type	Artificial short-circuit faults
	Fault location	Intra-phase and inter-phase winding sections
	Fault simulation	Controlled conductive bridging
Data acquisition	Measured quantities	Magnitude, Phase, Impedance, Impedance-phase
	Data format	Frequency-domain discrete samples
	Validation	Repeated measurements for consistency

Magnitude, phase, impedance, and impedance-phase responses were recorded for both healthy and faulted conditions. These measurements constituted the experimental dataset from which the multi-domain descriptors and MFDI values were subsequently obtained. The transformer specifications and the principal measurement conditions are summarized in Table 2.

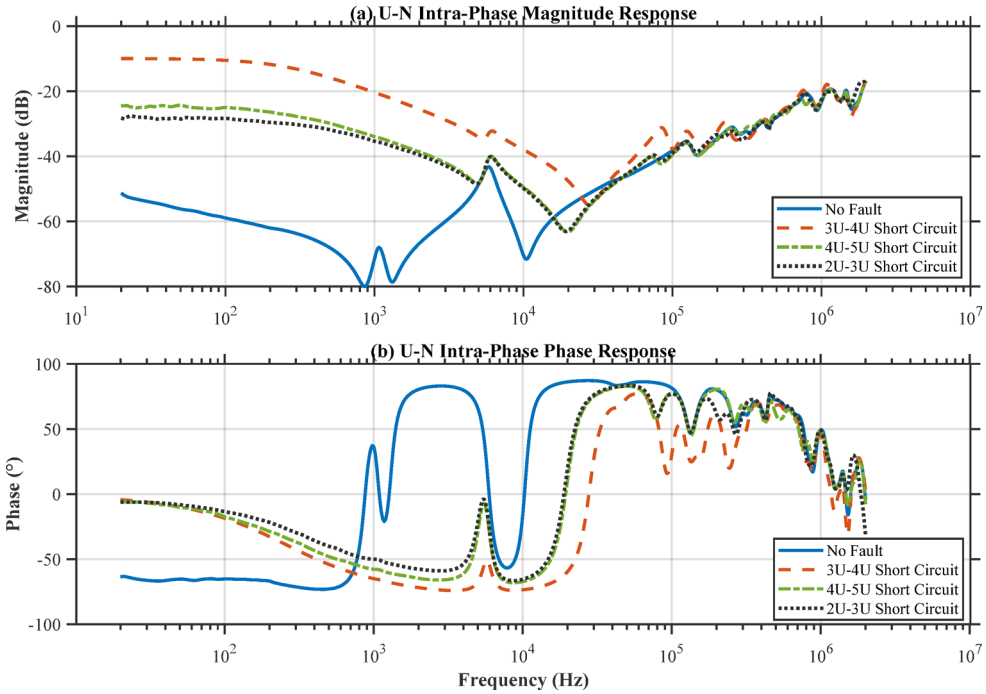


Fig. 5 U–N intra-phase SFRA responses under healthy and short-circuit conditions. (**a**) Magnitude response and (**b**) phase response as functions of frequency.

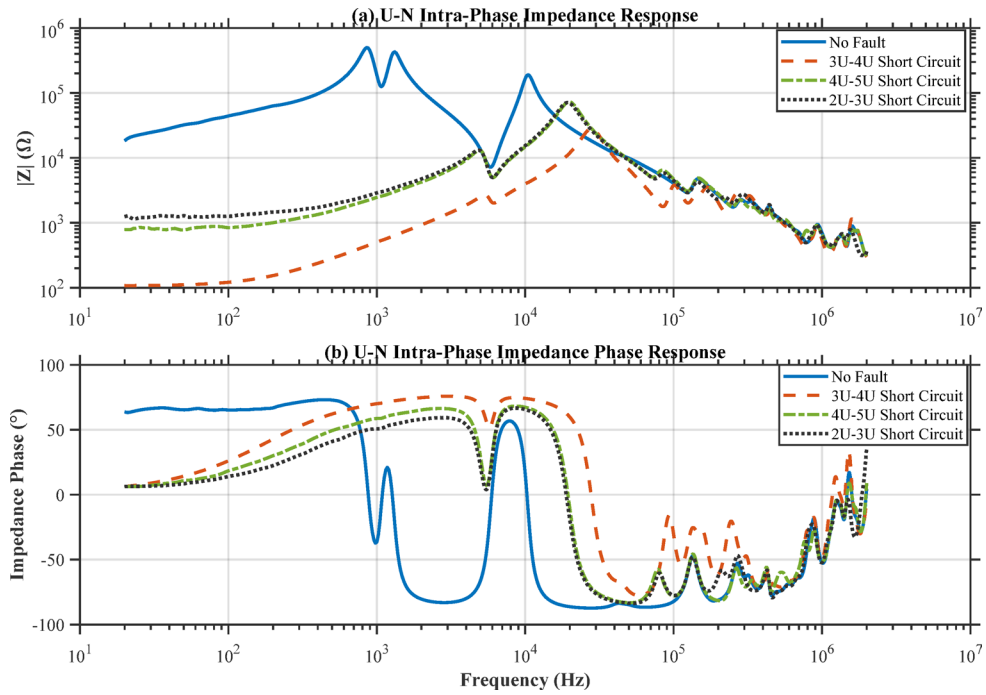


Fig. 6 U–N intra-phase impedance-based frequency responses. (**a**) Log–log impedance response and (**b**) impedance-phase response.

Intra-phase (U–N) fault analysis

The frequency responses of the transformer under intra-phase (U–N) condition are given in Figs. 5 and 6. The differences between the healthy and faulty conditions are most pronounced in the low and mid-frequency regions. These regions are closely related to the inductive structure of the winding and its overall structural properties.

These results indicate that intra-phase faults cause more localized changes in the winding structure. Therefore, their effects are particularly noticeable at low and medium frequencies. The smaller variations in the

high-frequency region indicate that inter-winding capacitive effects are less affected by these faults. This shows that focusing on a single frequency region in SFRA analysis is insufficient, and different frequency regions should be evaluated together, as the fault effects vary depending on both fault type and location.

Inter-phase (V–W) fault analysis

A different response pattern is observed for the inter-phase V–W case. As shown in Figs. 7 and 8, the 4 V–2 W short circuit produces substantial changes over a broader part of the frequency spectrum. Pronounced deviations are visible not only in magnitude and phase but also in the impedance and impedance-phase responses.

The broader spectral disturbance can be associated with the direct electrical interaction between two winding phases. Unlike the intra-phase cases, where the disturbance is confined to a section of one winding, the inter-phase short circuit modifies the electromagnetic coupling between separate windings. The resulting change therefore affects several response characteristics simultaneously and produces a more distinct departure from the healthy SFRA signature.

Comparative analysis of intra-phase and inter-phase fault behavior

The experimental responses indicate two different diagnostic situations. The intra-phase cases are characterized by relatively localized spectral changes and considerable similarity between fault signatures. The inter-phase case, in contrast, introduces broader changes across several SFRA response domains. The MFDI and machine-learning analyses were therefore examined together to determine how these physical differences are represented quantitatively.

Quantitative fault assessment using MFDI

Figure 9; Table 3 summarize the MFDI values calculated for the investigated conditions. The healthy responses produce values of 0.080 for U–N and 0.054 for V–W, whereas all short-circuit cases yield substantially larger

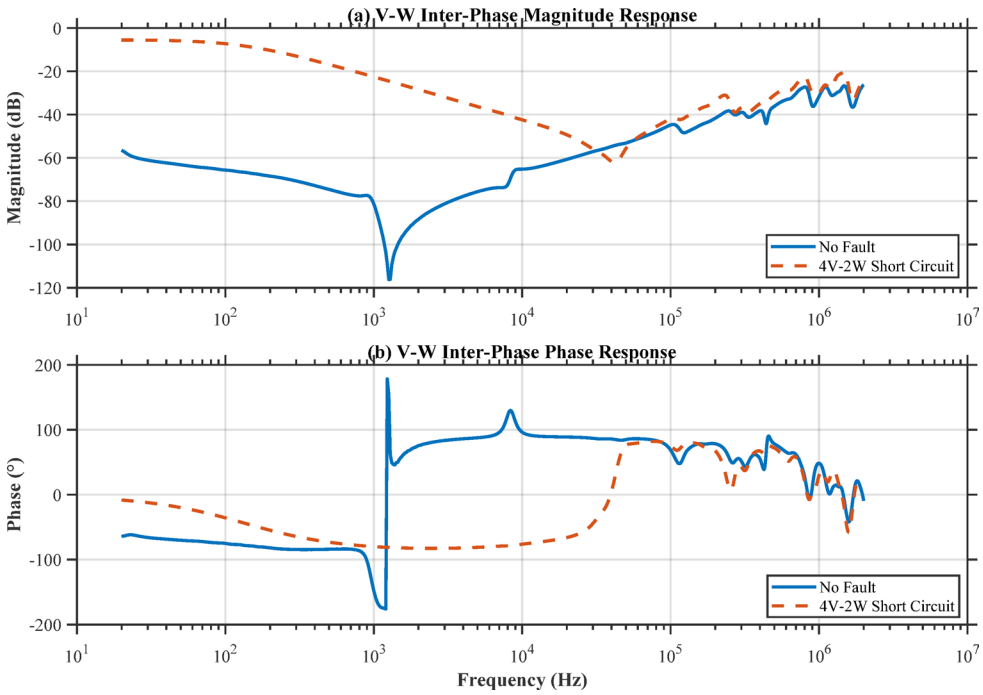


Fig. 7 V–W inter-phase SFRA responses comparing healthy and faulted conditions. (**a**) Magnitude response and (**b**) phase response.

https://doi.org/10.1038/s41598-026-72481-3

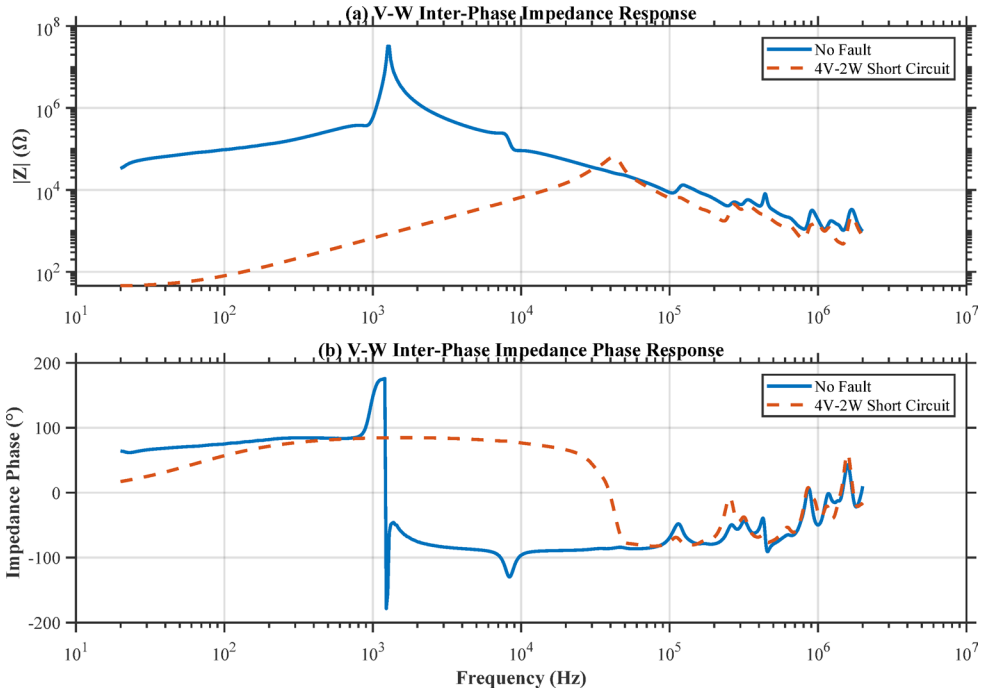


Fig. 8 V–W inter-phase impedance characteristics under fault conditions. (**a**) Logarithmic impedance response and (**b**) impedance-phase response.

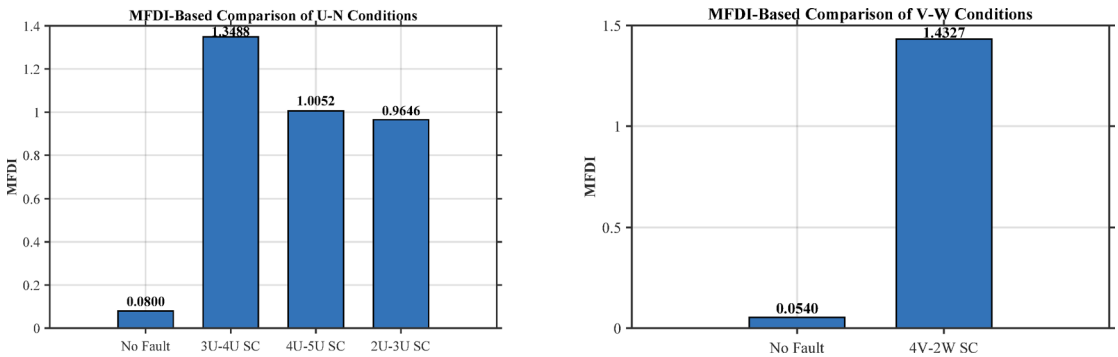


Fig. 9 MFDI comparison across transformer conditions.

Table 3 Advanced normalized Multi-Domain Fault Deviation Index for intra- and inter-phase fault conditions.

Intra-phase		Inter-phase	
Fault	MFDI value	Fault	MFDI value
Healthy condition	0.08	Healthy condition	0.054
2U–3U short circuit	0.9646		
4U–5U short circuit	1.0052	4 V–2 W short circuit	1.4327
3U–4U short circuit	1.3488		

values. Therefore, the index provides a clear numerical distinction between the healthy state and the fault conditions considered in the experiments.

Among the intra-phase cases, the MFDI values are 0.9646 for the 2U–3U short circuit, 1.0052 for 4U–5U, and 1.3488 for 3U–4U. The highest MFDI is therefore obtained for the short circuit involving the largest winding section. The greater number of affected turns may be one factor contributing to the larger change observed in the SFRA response. However, the number of turns alone does not explain the differences among the intra-phase cases. The 2U–3U and 4U–5U sections both contain 110 turns, yet their MFDI values are slightly different, at

0.9646 and 1.0052, respectively. This difference suggests that the location of the short-circuited section may also influence the frequency response. In this study, MFDI is therefore interpreted as a quantitative measure of deviation from the healthy SFRA response. It is not intended to represent a calibrated measure of mechanical fault severity.

The 4 V–2 W inter-phase short circuit shows a different response and produces the highest MFDI value of 1.4327. This fault establishes a direct electrical connection between two different phase windings, leading to broader changes in magnitude, phase, impedance, and impedance-phase responses. The higher MFDI value reflects the greater overall deviation of these responses from the healthy condition. No indication of MFDI saturation is observed for the fault conditions examined in this study.

The present experiments were not designed to establish the sensitivity limit of MFDI for incipient faults or progressively increasing mechanical deformation. The investigated conditions were deliberately introduced as controlled and repeatable short-circuit cases. Consequently, the response of the index to very small winding displacements or early-stage defects remains to be established experimentally. Therefore, future work should include controlled progressive fault levels so that the minimum detectable change and the suitability of MFDI for early fault detection can be assessed more directly.

Machine learning-based classification of transformer fault conditions

The multi-domain features were subsequently evaluated using SVM and Random Forest classifiers. Figure 10 presents the corresponding confusion matrices, while the main performance measures are listed in Table 4.

The intra-phase problem remains challenging. SVM achieved an accuracy of 52.08%, compared with 42.71% for Random Forest. Macro-precision, macro-recall, and macro-F1 values follow the same general trend. This level of performance is consistent with the measured SFRA responses: the three intra-phase short-circuit conditions modify only limited portions of the winding response, and their feature distributions consequently overlap. Misclassification among these cases is therefore not unexpected.

The machine-learning analysis was used to examine how well the extracted features distinguish the investigated fault conditions. It should therefore be regarded as a complementary evaluation of the MFDI-based feature space rather than as the sole diagnostic output of the framework. The moderate classification performance obtained for the intra-phase cases reflects the similarity of their SFRA signatures and the resulting overlap between classes. Despite this overlap, MFDI provides a quantitative measure of the changes observed in the SFRA response and preserves their physical interpretation.

A much clearer separation is obtained for the inter-phase case. SVM achieved an accuracy of 95.83%, and Random Forest correctly classified all V–W samples, giving 100% accuracy, macro-precision, macro-recall, and macro-F1. This improvement can be related to the broader spectral changes caused by the inter-phase short circuit. Changes occur simultaneously in several response domains, making the resulting feature patterns more distinct. The contrast between the intra-phase and inter-phase results suggests that classification performance is influenced primarily by the separability of the underlying SFRA signatures rather than by the choice of classifier alone.

To provide a direct comparison with conventional SFRA measures, Local MFDI was also evaluated against the Correlation Coefficient (CC), Absolute Sum of Logarithmic Error (ASLE), Euclidean Distance (ED), Standard Deviation (SD), and Comparative Standard Deviation (CSD). The same frequency-window segmentation and five-fold cross-validation procedure were used for all indices. Each index was represented by a single scalar feature to maintain a consistent basis for comparison.

As reported in Table 5, Local MFDI achieved 55.21% accuracy with both SVM and Random Forest for the U–N cases, giving the highest accuracy among the evaluated single-feature indices. For the V–W case, Local MFDI reached 100% accuracy with Random Forest. With SVM, ED and CSD achieved 87.50%, compared with 83.33% for Local MFDI. The results do not suggest that MFDI is superior under every classifier and fault condition. Instead, it shows that Local MFDI remains competitive and offers improved discrimination in the

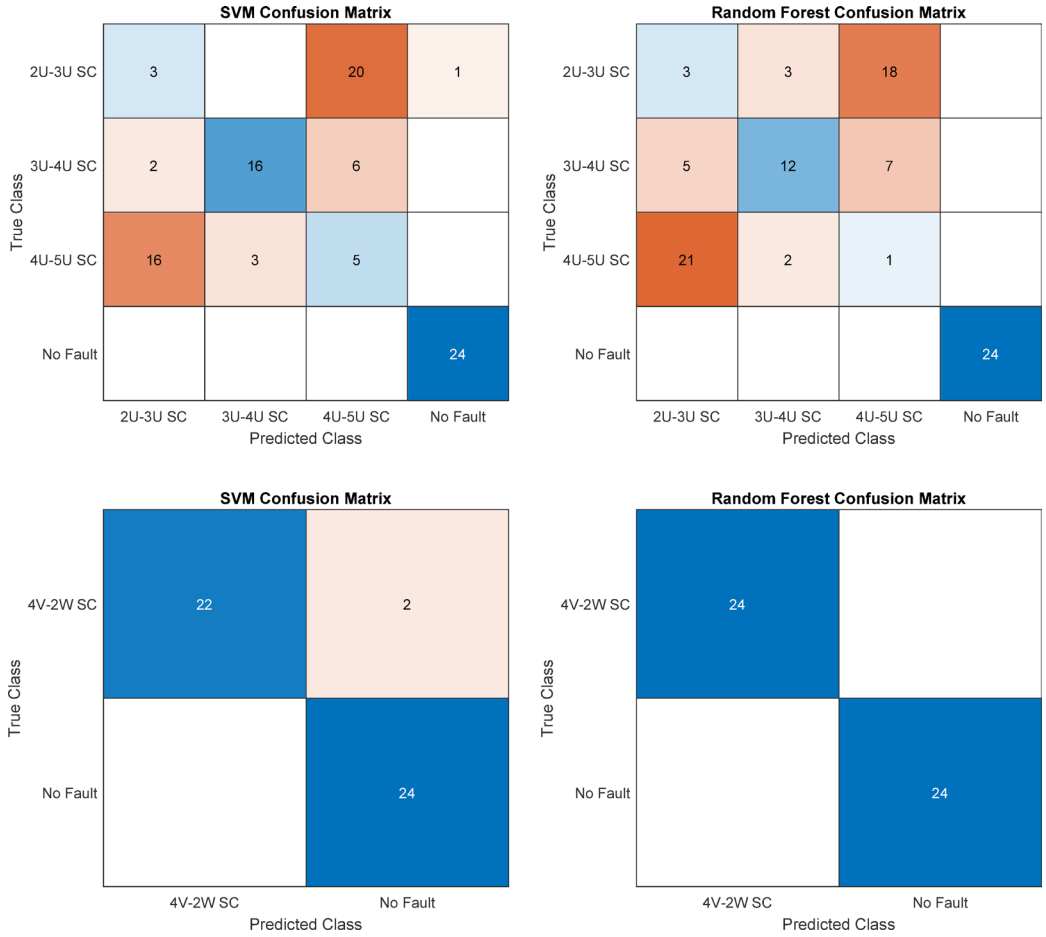


Fig. 10 Confusion matrix-based evaluation of classification performance using SVM and Random Forest models.

Table 4 Performance comparison of the SVM and Random Forest classifiers using the proposed multi-domain feature set.

Fault scenario	Classifier	Accuracy	Macro Precision	Macro Recall	Macro F1-score
Intra-phase (U–N)	SVM	52.08%	52.66%	52.08%	50.97%
	Random Forest	42.71%	46.19%	42.71%	43.46%
Inter-phase (V–W)	SVM	95.83%	96.15%	95.83%	95.83%
	Random Forest	100.00%	100.00%	100.00%	100.00%

Table 5 Classification accuracy comparison of conventional SFRA statistical indices and the proposed Local MFDI using a single-feature representation.

Feature	Intra-phase (U–N) SVM (%)	Intra-phase (U–N) RF (%)	Inter-phase (V–W) SVM (%)	Inter-phase (V–W) RF (%)
Correlation Coefficient (CC)	41.67	45.83	79.17	95.83
Absolute Sum of Logarithmic Error (ASLE)	44.79	40.63	81.25	97.92
Euclidean Distance (ED)	51.04	45.83	87.50	97.92
Standard Deviation (SD)	50.00	48.96	83.33	97.92
Comparative Standard Deviation (CSD)	46.88	42.71	87.50	95.83
Proposed Local MFDI	55.21	55.21	83.33	100.00

intra-phase problem while combining information from several SFRA response domains within one physically interpretable quantity.

Multi-domain feature space representation and analysis

To further analyze the structure and distinguishing characteristics of the obtained features, a multi-domain feature matrix was examined. Figure 11 shows the feature matrix for intra-phase and inter-phase faults. Each row represents a fault condition, and each column represents a feature obtained from a specific frequency band.

The variations between features are smaller and more dispersed in intra-phase faults. Although there are differences between fault types, similarities are observed in some regions. This indicates that distinguishing these faults from each other is more challenging. However, a much clearer separation emerges for the inter-phase fault scenario. Overall, the multi-domain feature matrix illustrates the distinct feature-space characteristics associated with the investigated intra-phase and inter-phase fault conditions.

In this study, the experimental validation was intentionally limited to representative intra-phase (U–N) and inter-phase (V–W) fault scenarios. These two fault types were selected because they represent two fundamentally different fault topologies, allowing the proposed MFDI framework to be evaluated under both localized and globally distributed winding disturbances. Although the proposed methodology is formulated independently of the fault type and can be applied to other winding defects that alter the SFRA response, such as axial displacement, radial deformation, hoop buckling, winding collapse, and inter-turn short circuits, comprehensive experimental validation for these additional fault scenarios remains part of future work.

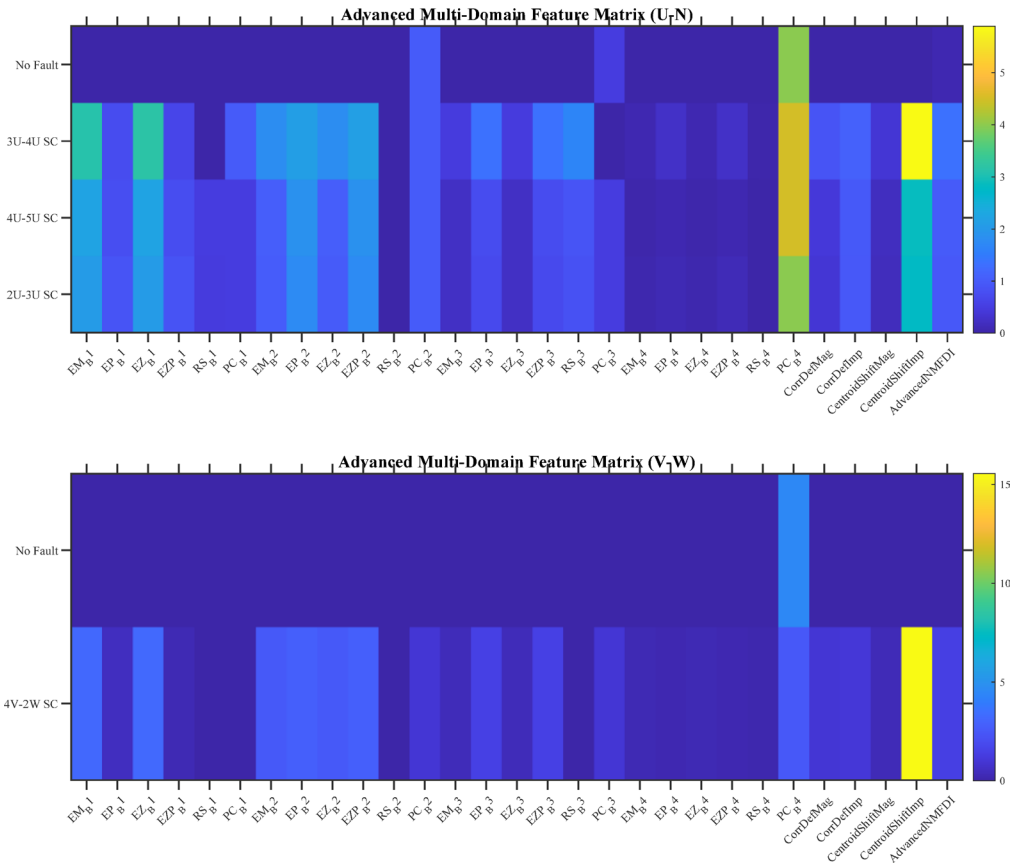


Fig. 11 Multi-domain feature matrix visualization for (**a**) intra-phase and (**b**) inter-phase transformer conditions.

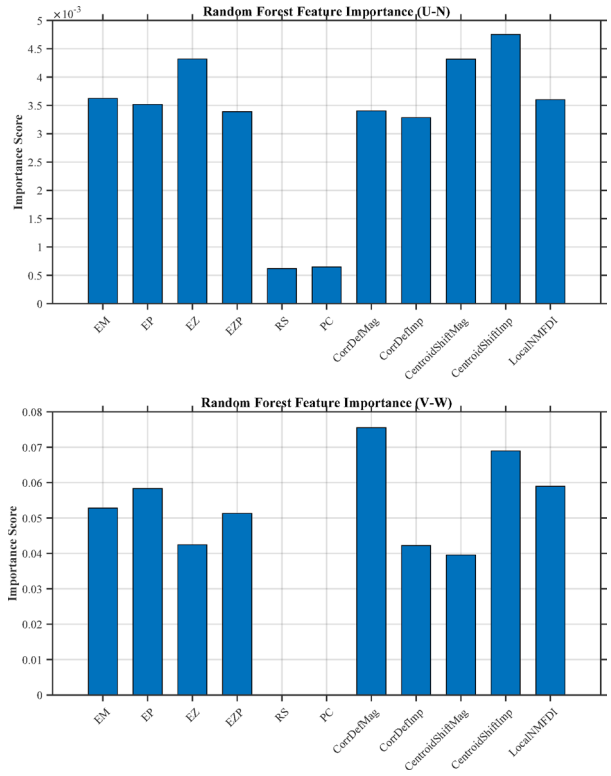


Fig. 12 Feature importance ranking obtained from the Random Forest model for (**a**) intra-phase and (**b**) inter-phase fault conditions.

Feature importance analysis using Random Forest

Random Forest feature importance was examined to identify which parts of the multi-domain representation contributed most strongly to classification. The resulting rankings are presented in Fig. 12.

For the intra-phase cases, importance is distributed across several descriptors rather than being dominated by a single feature. This distributed pattern is consistent with the relatively subtle nature of the U–N changes: no single response quantity is sufficient to distinguish all fault locations reliably, and classification depends on information drawn jointly from magnitude, phase, impedance, resonance, and related descriptors.

The inter-phase case exhibits a more concentrated importance pattern. Features associated with impedance variation, resonance behavior, and magnitude changes become more prominent in particular frequency regions. These features correspond to the larger electromagnetic disturbance already visible in the V–W frequency responses.

Taken together, the feature-importance results provide a physical interpretation of the classification behavior. The multi-domain formulation is most useful not because one descriptor consistently dominates, but because the relative contribution of individual features changes with the fault topology and the frequency region in which the disturbance appears.

Conclusion

This study presents a quantitative and measurement-oriented framework for transformer fault diagnosis based on the proposed advanced normalized Multi-Domain Fault Deviation Index (MFDI). This developed method evaluates magnitude, phase, impedance, and resonance-based characteristics together. This allows for a more systematic analysis of changes in frequency response. The experimental results demonstrate that the MFDI provides a clear and consistent separation between healthy and faulted conditions. For the intra-phase cases, the method captured relatively localized changes in the frequency response and provided quantitative differentiation among the investigated short-circuit conditions. Although the machine-learning classification performance remained moderate for these cases, the MFDI provided a physically meaningful and interpretable representation of the corresponding SFRA deviations.

Even more pronounced results are observed in the case of inter-phase faults. These faults induce stronger and more widespread disturbances in the transformer's electromagnetic structure. This behavior is consistently reflected in the MFDI values and is accompanied by high classification performance achieved using SVM and RF models. The combined evaluation of intra-phase and inter-phase faults clearly demonstrates the sensitivity of the proposed approach to different fault types. The proposed multi-domain feature combination approach successfully captures both cases, enabling a more comprehensive analysis of fault behavior.

In conclusion, the proposed framework supports a more quantitative, interpretable, and machine-learning-compatible application of SFRA for transformer winding condition assessment. Its physically meaningful feature representation and diagnostic capability indicate promising potential for future integration into intelligent transformer monitoring and predictive maintenance systems.

Author contributions C.K. and M.S.M. carried out the experiments. C.K. contributed to conceptualization, methodology, software development, validation, and writing of the original draft. M.S.M. contributed to methodology, validation, supervision, and writing—review & editing. M.A., M.K., and Z.Y. contributed to validation and writing—review & editing. All authors reviewed and approved the final manuscript.

Funding This study was supported by the Scientific and Technological Research Council of Türkiye (TÜBİTAK) under Project No. 123E658, and by the Scientific Research Projects Coordination Unit of Inonu University under Project No. FDP-2024-3702 and Project No. FBA-2026-4977.

Data availability The datasets generated and/or analyzed during the current study are available from the corresponding author on reasonable request at cemal.keles@inonu.edu.tr.

Declarations

Competing interests The authors declare no competing interests.

Open Access This article is licensed under a Creative Commons Attribution 4.0 International License, which permits use, sharing, adaptation, distribution and reproduction in any medium or format, as long as you give appropriate credit to the original author(s) and the source, provide a link to the Creative Commons licence, and indicate if changes were made. The images or other third party material in this article are included in the article's Creative Commons licence, unless indicated otherwise in a credit line to the material. If material is not included in the article's Creative Commons licence and your intended use is not permitted by statutory regulation or exceeds the permitted use, you will need to obtain permission directly from the copyright holder. To view a copy of this licence, visit http://creativecommons.org/licenses/by/4.0/.

References

1. Youssef, M., Abdelaziz, E., Mohamed, H. S. & Attia, M. Condition monitoring and fault diagnosis of power transformer based on non-invasive measurement. *Sci. Rep.* **15**, 32123 (2025).

2. Abbasi, A. R. Fault detection and diagnosis in power transformers: A comprehensive review and classification of publications and methods. *Electr. Power Syst. Res.* **209**, 107990 (2022).
3. Tenbohlen, S. et al. Diagnostic measurements for power transformers. *Energies* **9**, 347 (2016).
4. Keleş, C., Mamiş, M. S., Arkan, M. & Köseoğlu, M. Fault detection in power transformer windings using SFRA. In *Güç Sistemleri Konferansı IV* 1–4. (2025).
5. Vahedi, A. & Behjat, V. Online monitoring of power transformers for detection of internal winding short circuit faults using negative sequence analysis. *Eur. Trans. Electr. Power*. **21**, 196–211 (2011).
6. Ryder, S. A. Diagnosing transformer faults using frequency response analysis. *IEEE Electr. Insul. Mag*. **19**, 16–22 (2003).
7. Senobari, R. K., Sadeh, J. & Borsi, H. Frequency response analysis (FRA) of transformers as a tool for fault detection and location: A review. *Electr. Power Syst. Res.* **155**, 172–183 (2018).
8. Beheshti Asl, M., Fofana, I., Meghnefi, F., Brahami, Y. & Souza, J. P. D. C. A comprehensive review of transformer winding diagnostics: integrating frequency response analysis with machine learning approaches. *Energies* **18**, 1209 (2025).
9. Christopoulos, C. & Wright, A. *Electrical Power System Protection* (Springer Science & Business Media, 1999).
10. Alsuhaibani, S., Khan, Y., Beroual, A. & Malik, N. H. A review of frequency response analysis methods for power transformer diagnostics. *Energies* **9**, 879 (2016).
11. Samimi, M. H. & Tenbohlen, S. FRA interpretation using numerical indices: State-of-the-art. *Int. J. Electr. Power Energy Syst.* **89**, 115–125 (2017).
12. Akdağ, M., Keleş, C. & Mamiş, M. S. A novel method for detection of power transformer internal arcs using alternative transient program-electromagnetic transients program. In *European EMTP-ATP Users Group e.V.* 1–12. (2024).
13. Maseko, N. S., Thango, B. A. & Mabunda, N. Fault detection in power transformers using frequency response analysis. *Appl. Sci.* **15**, 2406 (2025).
14. Badgujar, K. P. & Gojiya, M. V. Capacitive cross-phase connection: a new test connection for SFRA test. *Trans. Indian Natl. Acad. Eng.* **8**, 661–670 (2023).
15. Mamiş, M. S., Ari, İ., Keleş, C. & Arkan, M. ATP-EMTP simulation of power transformers for detecting winding faults using sweep frequency response analysis. In *European EMTP-ATP Users Group e.V.* 1–15. (Lyon, France, 2025).
16. Dick, E. P. & Erven, C. C. Transformer diagnostic testing by frequency response analysis. *IEEE Trans. Power Appar. Syst.* **PAS-97**, 2144–2153 (1978).
17. Sreeram, V., Reddy, S. S., Gurudev, T., Maroti, M. & Rajkumar, M. Investigation into the correlation of SFRA numerical indices and short circuit reactance measurements of transformers. In *The International Conference on Machine Learning, Advances in Computing, Renewable Energy and Communication (MARC 2020)*) 567–576. (Ghaziabad, Uttar Pradesh, India, 2020).
18. Moradzadeh, A. Early detection of turn-to-turn faults in power transformer winding: an experimental study. In *2019 International Aegean Conference on Electrical Machines and Power Electronics (ACEMP) & 2019 International Conference on Optimization of Electrical and Electronic Equipment (OPTIM)* 199–204. https://doi.org/10.1109/ACEMP-OPTIM44294.2019.9007169 (IEEE, 2019).
19. Moradzadeh, A., Member, S. & Pourhossein, K. Locating inter-turn faults in transformer windings using isometric feature mapping of frequency response traces. *IEEE Trans. Ind. Inf.* **17**, 6962–6970 (2021).
20. Yoon, Y. et al. High-frequency modeling of a three-winding power transformer using sweep frequency response analysis. *Energies* **14**, 4009 (2021).
21. Li, Z., He, Y., Xing, Z. & Chen, M. Minor fault diagnosis of transformer winding using polar plot based on frequency response analysis. *Int. J. Electr. Power Energy Syst.* **152**, 109173 (2023).
22. Al-ameri, S. M. et al. Interpretation of frequency response analysis for fault diagnosis in power transformers. *Appl. Sci.* **11**, 2923 (2021).
23. Hosseini, A., Abbasi, A., Abbasi, A. R. & Mahmoudi, M. Transformer windings defects identification using frequency response analysis and advanced data visualization techniques. *Sci. Rep.* **15**, 40595 (2025).
24. Kornatowski, E. & Banaszak, S. Frequency response quality index for assessing the mechanical condition of transformer windings. *Energies* **13**, 29 (2020).
25. Rudin, C. Stop explaining black box machine learning models for high stakes decisions and use interpretable models instead. *Nat. Mach. Intell.* **1**, 206–215 (2019).
26. Roscher, R., Bohn, B., Duarte, M. F. & Garcke, J. Explainable machine learning for scientific insights and discoveries. *IEEE Access.* **8**, 42200–42216 (2020).
27. Zhao, Z. et al. Identification of power transformer winding mechanical fault types based on online IFRA by support vector machine. *Energies* **10**, 2022 (2017).
28. Zhang, Z., Gao, W., Kari, T. & Lin, H. Identification of power transformer winding fault types by hierarchical dimension reduction classifier based on online IFRA. *Energies* **11**, 2434 (2018).
29. Tahir, M. & Tenbohlen, S. Transformer winding condition assessment using frequency response analysis and intelligent classification. *Energies* **14**, 3227 (2021).

30. Tahir, M. & Tenbohlen, S. Transformer winding fault classification and condition assessment using FRA and machine learning. *Energies* **16**, 3714 (2023).
31. Moradzadeh, A. et al. Turn-to-turn short circuit fault localization in transformer winding via image processing and deep learning method. *IEEE Trans. Ind. Inf.* **18**, 4417–4426 (2022).
32. Qian, G. et al. Fault diagnosis method for transformer winding based on frequency response analysis. *Energies* **18**, 2290 (2025).
33. Çuhadaroğlu, H. & Uyaroğlu, Y. Detection of transformer faults: AI-supported machine learning application in sweep frequency response analysis. *Energies* **18**, 2481 (2025).
34. Parkash, C. & Abbasi, A. R. Transformer's frequency response analysis results interpretation using a novel cross entropy based methodology. *Sci. Rep.* **13**, 6604 (2023).
35. Huerta-rosales, J. R. et al. Short-circuited turn fault diagnosis in transformers by using vibration signals, statistical time features, and support vector machines on FPGA. *Sensors* **21**, 3598 (2021).
36. Azad, V. T., Afsharirad, H., Ghazijahani, H. A. & Safari, A. Scientific Reports Article in Press Graph-based analysis of frequency response measurements for assessment of winding faults in power autotransformers IN Graph-Based Analysis of Frequency Response IN. *Sci. Rep.* https://doi.org/10.1038/s41598-026-49048-3 (2026).
37. Abedin, T., Xu, H. & Uddin, S. The impact of K selection in K – fold cross-validation on bias and variance in supervised learning models. *Sci. Rep.* **16**, 6084 (2026).
38. Megger. *FRAX-Series Sweep Frequency Analyser User Guide* (Megger, 2022).

Publisher's note Springer Nature remains neutral with regard to jurisdictional claims in published maps and institutional affiliations.

Authors and Affiliations

Cemal Keleş[1] · Mehmet Salih Mamiş[1] · Müslüm Arkan[1] · Murat Köseoğlu[1] · Zehva Yalçınöz[1]

✉ Cemal Keleş
cemal.keles@inonu.edu.tr

[1] Department of Electrical and Electronics Engineering, Inonu University, Malatya, Turkey